Ultra-short echo time magnetic resonance imaging for detection of pulmonary arteriovenous malformation recanalization after coil embolization: a case report and a phantom study

Kohei Hamamoto, Emiko Chiba, Katsuhiko Matsuura, Tomohisa Okochi, Keisuke Tanno and Osamu Tanaka

Abstract

A pulmonary arteriovenous malformation (PAVM) is a direct connection between the pulmonary arteries and veins for which metallic coil transcatheter embolization is the standard of care. Detecting recanalization after PAVM treatment is crucial, but direct visualization with computed tomography or magnetic resonance imaging (MRI) is generally difficult. Here, we report a case of a recanalized PAVM that was directly detected with ultra-short echo time MRI. The detection of these signals in the coils was confirmed in a phantom study.

Introduction

Pulmonary arteriovenous malformations (PAVMs) are usually congenital but can also rarely be acquired. PAVMs are anomalous direct communications between the pulmonary arterial and venous circulations through a thin-walled aneurysmal sac (1,2). Endovascular treatment with metallic coil embolization has been accepted as the standard of care for PAVM (2,3). However, recanalization is one of the concerns after embolization because some patients can develop neurologic events (4,5). Digital subtraction angiography (DSA) is the most reliable modality for detecting recanalization, but this is an invasive procedure. In recent years, computed tomography (CT) and magnetic resonance imaging (MRI) with or without contrast agents have become important in the evaluation of PAVM patency due to the non-invasiveness of these techniques (6–12). However, the direct visualization of recanalization through the coils is difficult with CT and MRI because of the prominent streaks or susceptibility artifacts from the metallic coils. This report describes the non-invasive direct visualization of the recanalization of a PAVM using ultra-short echo time (UTE) MRI. We also performed a phantom study to elucidate the capability of UTE MRI for the detection of signals in the coil.

Case report

A 22-year-old woman with a chest X-ray abnormality was referred to our department for further evaluation and treatment. She was diagnosed with hereditary hemorrhagic telangiectasia based on the Curacao criteria (13). A contrast-enhanced CT revealed one complex

Department of Radiology, Saitama Medical Center, Jichi Medical University, Saitama, Japan

Corresponding author:
Kohei Hamamoto, Department of Radiology, Saitama Medical Center, Jichi Medical University, 1-847 Amanuma-cho, Omiya-ku, Saitama 330-8503, Japan.
Email: hkouhei917@gmail.com

type PAVM with three feeding arteries in the left upper lobe (segment 1 + 2) of the lung and two simple type PAVMs in the right lower lobe (segment 10) of the lung. The diameters of the feeding arteries and the aneurysmal sacs of the PAVMs were as follows: (i) in the left upper lobe lesion, the diameters of the three feeding arteries and the aneurysmal sac were 3.9, 1.0, 1.6, and 5.3 mm; (ii) in the first right lower lobe lesion, the diameters of the feeding artery and aneurysmal sac were 3.0 and 3.6 mm, respectively; and (iii) in the second right lower lobe lesion, the diameters of the feeding artery and aneurysmal sac were 1.2 and 1.5 mm, respectively.

Transcatheter embolization of the feeding arteries and the aneurysmal sacs with 0.012- and 0.014-inch platinum coils, respectively, were performed and resulted in the complete occlusion of each of the PAVMs (Fig. 1). On follow-up unenhanced CT four months after the first procedure, the diameter of the aneurysmal sac of the PAVM in the left upper lobe decreased to 4.3 mm. However, visualization of the aneurysmal sac was quite limited, and evaluation of the continuity among the feeding artery, aneurysmal sac, and draining vein was not possible because of severe streak artifacts from the metallic coils (Fig. 2a and b). The aneurysmal sacs of the two lesions in the right lower lobe had resolved on follow-up CT, but definite confirmation of complete occlusion was difficult for the same reasons.

For further evaluation of the recanalization, we conducted UTE MRI and time-resolved contrast-enhanced magnetic resonance angiography (TR-CEMRA) using a 3.0-T MRI system (Vantage Titan 3T, Canon Medical Systems, Tochigi, Japan). The MRI parameters are listed in Table 1. For the UTE MRI, respiratory triggering applied at the beginning of expiration. Regarding the PAVM in the left upper lobe, UTE MRI enabled a clear visualization of the continuity of the main lateral feeding artery, the aneurysmal sac, and the draining vein (Fig. 2c and d), as well as the continuity between the medial feeding artery and the aneurysmal sac. On TR-CEMRA, the feeding artery and the
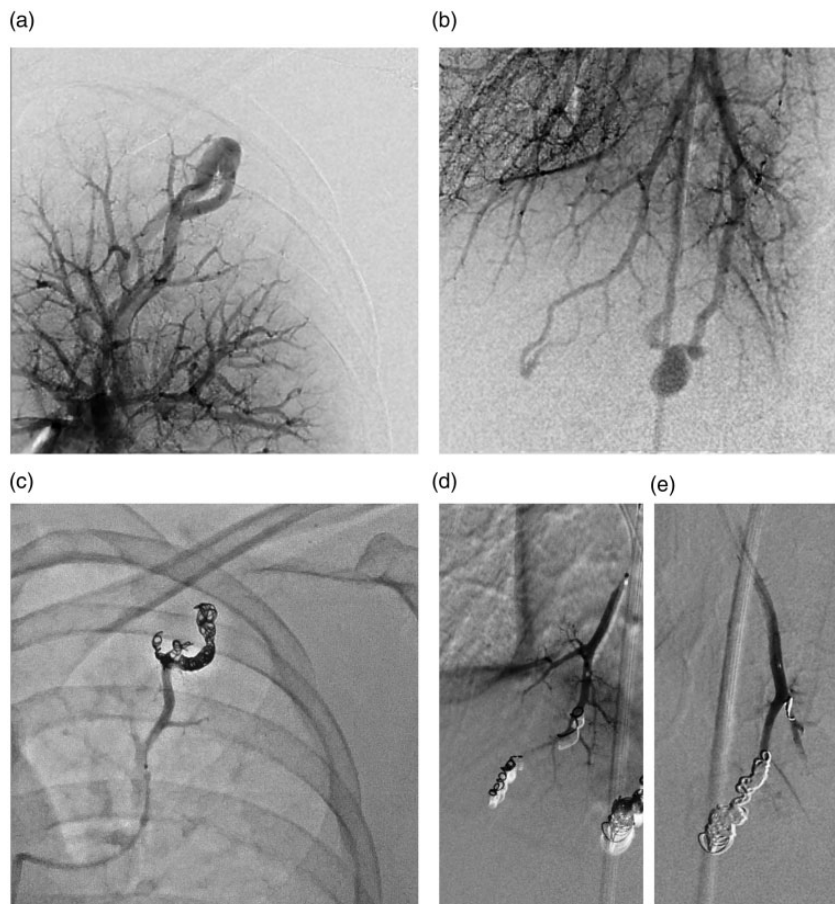

Fig. 1. Transcatheter coil embolization. (a) A complex-type PAVM with three feeding arteries and (b) two simple-type PAVMs in the left upper lobe (segment 1 + 2) and the right lower lobe (both segment 10), respectively. (c, d, e) After embolization of each feeding artery, no residual shunting was observed. PAVM, pulmonary arteriovenous malformation.
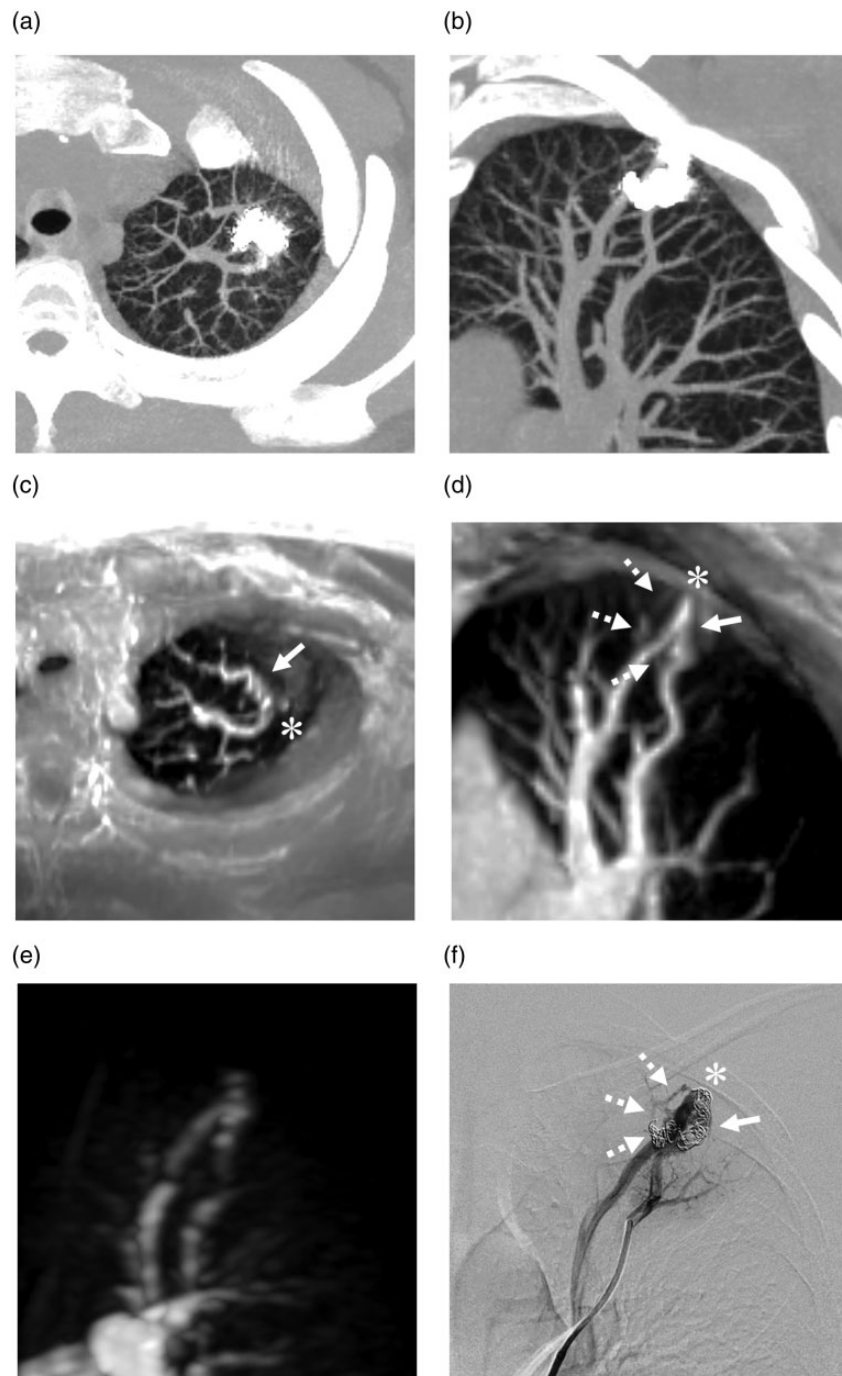
Fig. 2. Evaluation of recanalization after the first embolization of a pulmonary arteriovenous malformation (PAVM) in the left upper lobe. Unenhanced computed tomography with partial maximum intensity projection (MIP) (a, axial image; b, oblique coronal image) for image evaluation around the placed coils is difficult due to prominent streak artifact from the coils. Ultra-short echo time magnetic resonance image with partial MIP (c, axial image; d, oblique coronal image) showing the continuity of the lateral (arrows) and medial (dashed arrows) feeding arteries, aneurysmal sac (asterisk), and draining vein in the PAVM. Note that the signals in the coils are clearly visualized on UTE MRI. (e) On time-resolved contrast-enhanced magnetic resonance angiography with MIP (oblique coronal image), simultaneous visualization of the feeding artery and draining vein in the pulmonary arterial phase is achieved. (f) On digital subtraction angiography, recanalization through the previously placed coils is noted (arrow and dashed arrows). The asterisk indicates the aneurysmal sac.

Table 1. MRI parameters.

	Patient		Phantom
	UTE MRI	TR-CEMRA	UTE MRI
TE/TR (ms)	0.096/3.7	1.3/3.7	0.096/3.7
Flip angle (°)	5	20	5
Slice thickness (mm)	1	1.25*	1
Slice section (n)	200 (to cover the entire lung field)	40 (to cover the embolized lesions)	40
Field of view (mm)	480 × 480	370 × 370	240 × 240
Matrix size	512 × 512	512 × 320†	304 × 304
Signal acquired (n)	1	1	1
Parallel imaging acceleration factor	N/A	2	N/A
Acquisition voxel size (mm)	0.94 × 0.94 × 1	0.72 × 1.16 × 1.25	0.76 × 0.76 × 1
Imaging time	7 min 50 s	30 s	2 min 30 s

*The acquired slice sections of 2.5 mm were reconstructed with 1.25-mm voxel intervals by means of mid-slice reconstruction.
†Reconstruction matrix.
N/A, not applicable.

draining vein were simultaneously visualized (Fig. 2e) in the pulmonary arterial phase, which suggested recanalization. However, the continuity between the feeding arteries and the aneurysmal sac was unclear on TR-CEMRA. In both PAVMs in the right lower lobe, UTE MRI revealed resolutions of the aneurysmal sacs and the draining veins, and TR-CEMRA did not reveal any enhancement of the aneurysmal sacs or the draining veins in the pulmonary arterial phase, which indicated complete occlusion. Based on these findings, recanalization through the placed coils in the PAVM in the left upper lobe was suggested.

DSA was applied as a secondary intervention and confirmed the recanalization through the coils placed in the lateral and medial feeding arteries (Fig. 2f) of the left upper lobe PAVM. These findings were quite similar to those yielded by UTE MRI. An additional platinum coil embolization of the remnant lumen was achieved. In contrast, the complete occlusions of both PAVMs in the right lower lobe were confirmed on DSA.

The imaging findings of the present case suggested that UTE MRI can detect MR signals in the coils. Therefore, we assessed the capability of this sequence to detect signals in a coil using a coil phantom. A 0.015-inch bare platinum coil (IDC, Boston Scientific Japan Co. Ltd., Tokyo, Japan) with a diameter of 8 mm and a length of 20 cm was placed in a tube that had a range of 15 mm (Fig. 3a). The tube was embedded in 1.5% agarose gel and was connected to a continuous flow pump. This coil phantom was perfused with normal saline at a flow velocity of 15 cm/s. UTE images were acquired with the parameters listed in Table 1. The image data were transferred to a workstation (Ziostation2, Ziosoft,

Tokyo, Japan) that was equipped with a multi-planar reconstruction algorithm for the source images. As shown in Fig. 3b and c, the signal in the placed coils was clearly visualized on UTE MRI. These findings were quite similar with produced with DSA (Fig. 3d).

Discussion

Assessment of PAVM patency after embolization is crucial because recanalization can occur in up to 50% of cases and cause neurologic events that are similar to those associated with untreated lesions (4,5). DSA remains the gold standard for identifying recanalization; however, in recent years, CT and MRA with or without contrast agents have been generally performed for the assessment of recanalization in embolized PAVMs because of their non-invasiveness (6–12). The detections of recanalization using unenhanced CT, contrast-enhanced CT, and TR-CEMRA have been reported to have sensitivities of 93%, 82%, and 93–100%, respectively, and specificities of 53%, 100%, and 93–100%, respectively (9,11). More recently, Hamamoto et al. demonstrated the high sensitivity and specificity (both 100%) of unenhanced MRA utilizing the time-spatial inversion pulse technique (time-SLIP MRA) in the detection of PAVM recanalization (12). However, the diagnostic criteria for recanalization that were used in these studies were based on morphologic changes and hemodynamic information; therefore, the sufficiency of these modalities for detecting recanalization of embolized PAVMs was not confirmed.

Achieving a definitive diagnosis of recanalization requires the visualization of the continuity of the feeding
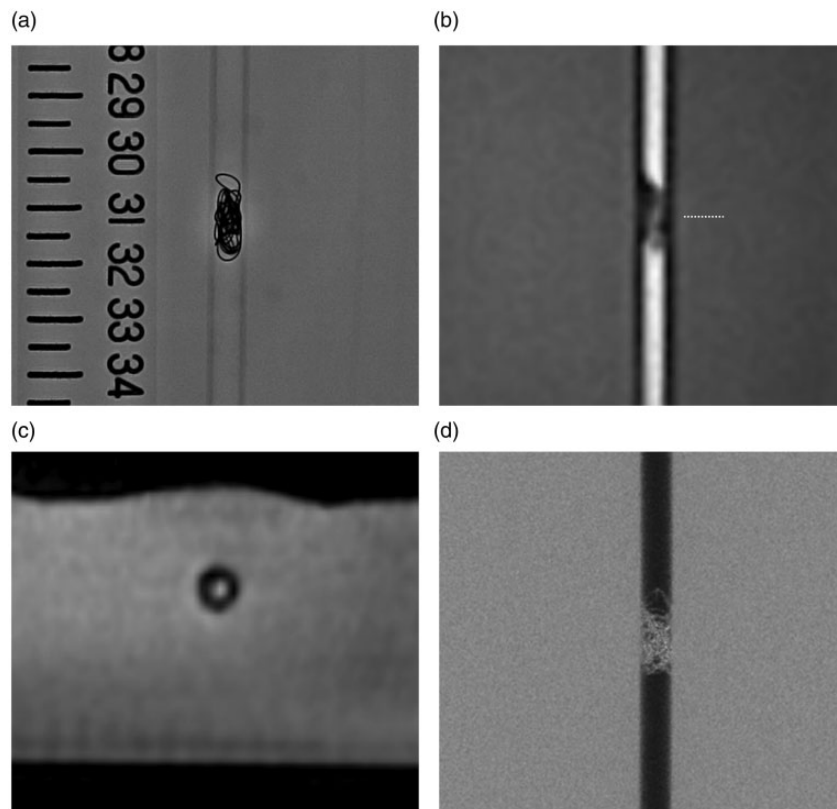
Fig. 3. Ultra-short echo time magnetic resonance imaging (UTE MRI) in a coil phantom. (a) X-ray image of the coil phantom. The signals in the coils are clearly visualized on UTE MRI with multi-planar reconstruction (b, coronal image; c, axial image corresponding to the site indicated by the dashed line in b). (d) Digital subtraction angiography image.

artery, aneurysmal sac, and draining vein through the placed coils. Acquisition of this evidence by CT and MRA is generally difficult because of the prominent streak or susceptibility artifacts from the metallic coils. In the present case, UTE MRI enabled the clear visualization of the continuity through the embolized coils from the feeding artery to the draining vein on images that were quite similar to those produced with DSA. Notably, UTE MRI acquired the signals in coils that were deployed with a high packing density. The capability of UTE MRI for detecting signals in the coil was confirmed with the coil phantom. These findings indicated that UTE MRI can provide useful information for the non-invasive definitive diagnosis of recanalization. To our best knowledge, this is the first report to demonstrating the utility of UTE MRI in the detection of the recanalization of embolized PAVMs.

The UTE (TE = 0.096 ms) is the most important feature of this sequence. UTE imaging can reduce magnetic susceptibility and enable the visualization of short T2 tissues, such as the musculoskeletal tissues, carotid plaques, and lung parenchyma (14–16). Additionally, UTE can minimize signal loss in the voxel space that is caused by phase dispersion due to disturbed blood flow, which may contribute to decreased magnetic

susceptibility. Consequently, the artifacts from the coils are diminished, and this change enables the visualization of signals in the coils. Similar to the present report, recent clinical studies have reported that UTE alone and UTE with the arterial spin labeling technique reduce the artifacts that are typically observed after coil or stent placement (17–19).

UTE MRI has additional advantages compared with CT, TR-CEMRA, and time-SLIP MRA. First, this method does not necessitate exposure to ionizing radiation or the risks associated with iodine- or gadolinium-based contrast agents, which nephrotoxicity, anaphylaxis, nephrogenic systemic fibrosis, and tissue deposition of gadolinium. Second, the relatively brief acquisition window in the late expiration phase that is triggered by respiratory gating enables high spatial and temporal resolution imaging and a reduction in motion artifacts compared with the settings for TR-CEMRA (20). Indeed, in the present case, UTE MRI was able to detect recanalization of a small vessel that was less than 1 mm in diameter (Fig. 2). Finally, UTE MRI can scan the entire lung field with high spatial resolution during a single session, whereas the numbers of acquisitions that are possible in a single session with time-SLIP MRA and TR-CEMRA are limited, which makes

imaging of the entire lung field difficult (11,12). However, theoretically, UTE MRI might visualize static tissues, such as thrombi in coils, as lesions with high signal intensity. Therefore, at the present stage of development of UTE MRI, imaging modalities, including TR-CEMRA and time-SLIP MRA, which provide hemodynamic information are still necessary to evaluate recanalization. This drawback may be avoidable with the combined use of the arterial spin labeling method, which can cancel the signal intensity from static tissue. Furthermore, the capability of UTE MRI to detect signals is thought to depend on the packing density of the coils and the materials that compose the embolic agents. Further investigations are warranted to clarify these issues.

In conclusion, this case report and the preliminary results of the phantom study suggest that UTE MRI is a useful method for detecting recanalization of PAVMs after coil embolization.

References

1. Remy J, Remy-Jardin M, Wattinne L, et al. Pulmonary arteriovenous malformations: evaluation with CT of the chest before and after treatment. Radiology 1992;182:809–816.
2. White RI Jr, Pollak JS, Wirth JA. Pulmonary arteriovenous malformations: diagnosis and transcatheter embolotherapy. J Vasc Interv Radiol 1996;7:787–804.
3. Mager JJ, Overtoom TT, Blauw H, et al. Embolotherapy of pulmonary arteriovenous malformations: long-term results in 112 patients. J Vasc Interv Radiol 2004;15:451–456.
4. Lee DW, White RI Jr, Egglin TK, et al. Embolotherapy of large pulmonary arteriovenous malformations: longterm results. Ann Thorac Surg 1997;64: 930–939. (discussion 939–940).
5. Milic A, Chan RP, Cohen JH, et al. Reperfusion of pulmonary arteriovenous malformations after embolotherapy. J Vasc Interv Radiol 2005;16:1675–1683.
6. Remy-Jardin M, Dumont P, Brillet PY, et al. Pulmonary arteriovenous malformations treated with embolotherapy: helical CT evaluation of long-term effectiveness after 2–21-year follow-up. Radiology 2006;239:576–585.
7. Fidelman N, Gordon RL, Bloom AI, et al. Reperfusion of pulmonary arteriovenous malformations after successful embolotherapy with vascular plugs. J Vasc Interv Radiol 2008;19:1246–1250.
8. Woodward CS, Pyeritz RE, Chittams JL, et al. Treated pulmonary arteriovenous malformations: patterns of persistence and associated retreatment success. Radiology 2013;269:919–926.
9. Makimoto S, Hiraki T, Gobara H, et al. Association between reperfusion and shrinkage percentage of the aneurysmal sac after embolization of pulmonary arteriovenous malformation: evaluation based on contrast-enhanced thin-section CT images. Jpn J Radiol 2014;32: 266–273.
10. Boussel L, Cernicanu A, Geerts L, et al. 4D time-resolved magnetic resonance angiography for noninvasive assessment of pulmonary arteriovenous malformations patency. J Magn Reson Imaging 2010;32:1110–1116.
11. Kawai T, Shimohira M, Kan H, et al. Feasibility of time-resolved MR angiography for detecting recanalization of pulmonary arteriovenous malformations treated with embolization with platinum coils. J Vasc Interv Radiol 2014;25:1339–1347.
12. Hamamoto K, Matsuura K, Chiba E, et al. Feasibility of non-contrast-enhanced MR angiography using the time-SLIP technique for the assessment of pulmonary arteriovenous malformation. Magn Reson Med Sci 2016;15: 253–265.
13. Shovlin CL, Guttmacher AE, Buscarini E, et al. Diagnostic criteria for hereditary hemorrhagic telangiectasia (Rendu-Osler-Weber syndrome). Am J Med Genet 2000;91:66–67.
14. Robson MD, Gatehouse PD, Bydder M, et al. Magnetic resonance: an introduction to ultrashort TE (UTE) imaging. J Comput Assist Tomogr 2003;27:825–846.
15. Bergin CJ, Pauly JM, Macovski A. Lung parenchyma: projection reconstruction MR imaging. Radiology 1991; 179:777–781.
16. Chan CF, Keenan NG, Nielles-Vallespin S, et al. Ultrashort echo time cardiovascular magnetic resonance of atherosclerotic carotid plaque. J Cardiovasc Magn Reson 2010;12:17.
17. Gönner F, Heid O, Remonda L, et al. MR angiography with ultrashort echo time in cerebral aneurysms treated with Guglielmi detachable coils. Am J Neuroradiol 1998; 19:1324–1328.
18. Gönner F, Lövblad KO, Heid O, et al. Magnetic resonance angiography with ultrashort echo times reduces the artefact of aneurysm clips. Neuroradiology 2002;44: 755–758.
19. Irie R, Suzuki M, Yamamoto M, et al. Assessing blood flow in an intracranial stent: A feasibility study of MR angiography using a silent scan after stent assisted coil embolization for anterior circulation aneurysms. Am J Neuroradiol 2015;36:967–970.
20. Vasbinder GB, Maki JH, Nijenhuis RJ, et al. Motion of the distal renal artery during three-dimensional contrast-enhanced breath-hold MRA. J Magn Reson Imaging 2002;16:685–696.